129900-1-F

Final Report

TECHNIQUES FOR THE EXTRACTION OF WATER DEPTH INFORMATION FROM LANDSAT DIGITAL DATA

DAVID R. LYZENGA, FABIAN C. POLCYN
Applications Division

MARCH 1979

Prepared for:
Defense Mapping Agency
Hydrographic/Topographic Center
Washington, DC 20315
Contract DMA 800-77-C-0053
Technical Monitor: James Hammack
Advanced Technology Division
System and Techniques Directorate

ENVIRONMENTAL
RESEARCH INSTITUTE OF MICHIGAN
FORMERLY WILLOW RUN LABORATORIES THE UNIVERSITY OF MICHIGAN
BOX 8618 • ANN ARBOR • MICHIGAN 48107

TECHNICAL REPORT STANDARD TITLE PAGE

1. Report No.	2. Government Accession No.	3. Recipient's Catalog No.
129900-1-F		

4. Title and Subtitle
TECHNIQUES FOR THE EXTRACTION OF WATER DEPTH INFORMATION FROM LANDSAT DIGITAL DATA

5. Report Date
MARCH 1979

6. Performing Organization Code

7. Author(s)
DAVID R. LYZENGA AND FABIAN C. POLCYN

8. Performing Organization Report No.
129900-1-F

9. Performing Organization Name and Address
Environmental Research Institute of Michigan
Applications Division, P.O. Box 8618
Ann Arbor, MI 48107

10. Work Unit No.

11. Contract or Grant No.
DMA 800-77-C-0053

12. Sponsoring Agency Name and Address
Defense Mapping Agency
Hydrographic/Topographic Center
Washington, D.C. 20315

13. Type of Report and Period Covered
Final Report
July 1977-September 1978

14. Sponsoring Agency Code

15. Supplementary Notes
Project Monitors: James Hammack, Advanced Technology Division
John Spinning, Systems and Techniques Directorate, DMA

16. Abstract

Landsat CCT data has potential for use in construction of shallow seas bathymetric charts. Special attention must be paid to the radiometric and geometric properties of the NASA supplied tapes to extract most accurate data. Various methods for destriping tape date have been tried depending on nature of Landsat scene and local variations of striping pattern. Geometric corrections using ground control points should be used but scene correction should be performed only once as final step to avoid loss of radiometric accuracy. Multidate Landsat data has multiple value for improving SNR, editing clouds and turbidity patterns and providing information on water clarity and bottom reflectance changes. Tests of water depth predictions from Landsat as compared to ship measurements show importance of bottom reflectance variations. Two channel techniques show promise and average reflectance values for Landsat pixels require further investigation.

17. Key Words	18. Distribution Statement
Remote Bathymetry Landsat Charting	

19. Security Classif. (of this report)	20. Security Classif. (of this page)	21. No. of Pages	22. Price
UNC	UNC	iii + 57	

ERIM

TABLE OF CONTENTS

LIST OF FIGURES

LIST OF TABLES

TECHNIQUES FOR THE EXTRACTION OF WATER DEPTH INFORMATION FROM LANDSAT DIGITAL DATA

1 INTRODUCTION

This report was prepared under contract DMA800-77-C-0053 as part of a continuing program supported by the Defense Mapping Agency, Hydrographic/Topographic Center for the exploitation of Landsat data for updating ocean charting of the world. Particular emphasis has been placed on developing computer techniques to best calculate and extract reliable water depth measurements from NASA supplied digital data taken from Landsat sensors over the shallow seas that are hazardous to shipping. Previous demonstrations of the feasibility of using Landsat digital data has been reported in the DMA sponsored report entitled "Demonstration of Satellite Bathymetric Mapping", ERIM Report No. 122200-1-F, 1977. In order to extract the measurement of water depth most accurately special attention must be paid to the radiometric and geometric properties of the Landsat sensor data as well as the correction of certain signal variations in the 6 detector arrays used to scan the oceans.

Furthermore, in order to reduce the effects of variable radiance contributions to the received signal from atmospheric and oceanic sources an investigation of multispectral and multitemporal techniques was begun during this period. Finally, a test of water depth accuracies as extracted from Landsat data using algorithms developed to date was made based on measurements taken aboard the R/V Constance in October 1977 in the Bahamian photo-bathymetric test range defined by John Spinning and James Hammack of the Advanced Technology Division, Systems and Techniques Directorate, Hydrographic and Topographic Center, DMA.

The progress to date (September 1978) on each of six tasks is reported in the following sections.

2
TASK 1 - RADIOMETRIC CORRECTIONS

The six-detector scanning configuration used in the Landsat multispectral scanner subsystem has resulted in continuing problems due to calibration differences among the detectors. These problems are caused mainly by variations in detector response characteristics, but are compounded by the system design and processing procedures used at NASA/Goddard. In this section, the discussion will focus on some of the algorithms which have been developed for reducing the striping problems in Landsat data sets which have been routinely processed and distributed by NASA. In the following section, the NASA processing procedures will be discussed, and recommendations will be made for modifying these procedures or for implementing alternative procedures which are more suitable for bathymetric applications.

Several different types of destriping algorithms have been developed, each with its own advantages and disadvantages. The simplest type of algorithm is an offset correction, in which a constant c_i is added to the signals for detector i (i = 1, 6) in order to minimize the variance of the entire data set. The second type of algorithm, in order of complexity, is a correction of the form

$$V'_i = a_i V_i + b_i$$

where V'_i is the corrected signal for detector i, V_i is the uncorrected signal, and a_i and b_i are parameters which may be interpreted as correction factors for differences in gain and offset, respectively, among the detectors. This algorithm can, in principle, correct for detector differences over a wider range of signals than the simple offset correction, assuming that the detector responses are linear with radiance. A modification of this algorithm applies a piecewise linear correction to each detector, on the assumption that the detector responses

are nonlinear but may be approximated by a piecewise linear function. The third type of algorithm is one which replaces each signal value by a corrected value using a lookup table. This procedure is capable of making any kind of linear or nonlinear correction and is, therefore, the most general type of algorithm.

An important criterion in evaluating the various types of destriping algorithms is the accuracy with which the correction parameters can be determined for a given scene. For all but the simple offset correction, the determination of these parameters requires that the scene must contain areas of a uniform or a slowly varying signal over a wide range of signals. These conditions do not occur in some oceanic scenes, for example those containing large expanses of open water and only a few reefs or shoals. For such scenes, the offset correction is the only useable method since the parameters required for the other algorithms cannot be accurately determined. Fortunately, an offset correction with parameters determined from the open water signal is usually adequate for water depth processing, since the sensitivity to noise is greatest for signal values near the deep water signal.

A second factor to be considered in selecting a destriping algorithm is the possibility of variations in the striping pattern from one part of the scene to another. This effect is illustrated in Figure 1, which shows mean values for each detector over open water in two different parts of Landsat frame 11249-14435. The areas each contain a total of 6000 pixels (1000 pixels per detector), and are separated by 720 lines. The difference in the striping patterns for these two areas is most evident in MSS5; in area A, detectors 1 and 2 are about 1 count above the mean, while in area B, detector 1 is high and detectors 3 and 4 are about 1 count below the mean. An optimum striping correction for area B actually increases the variance among detectors for area A. In order to remove the striping from the entire scene, the scene must be broken into subregions within which the striping pattern is uniform within

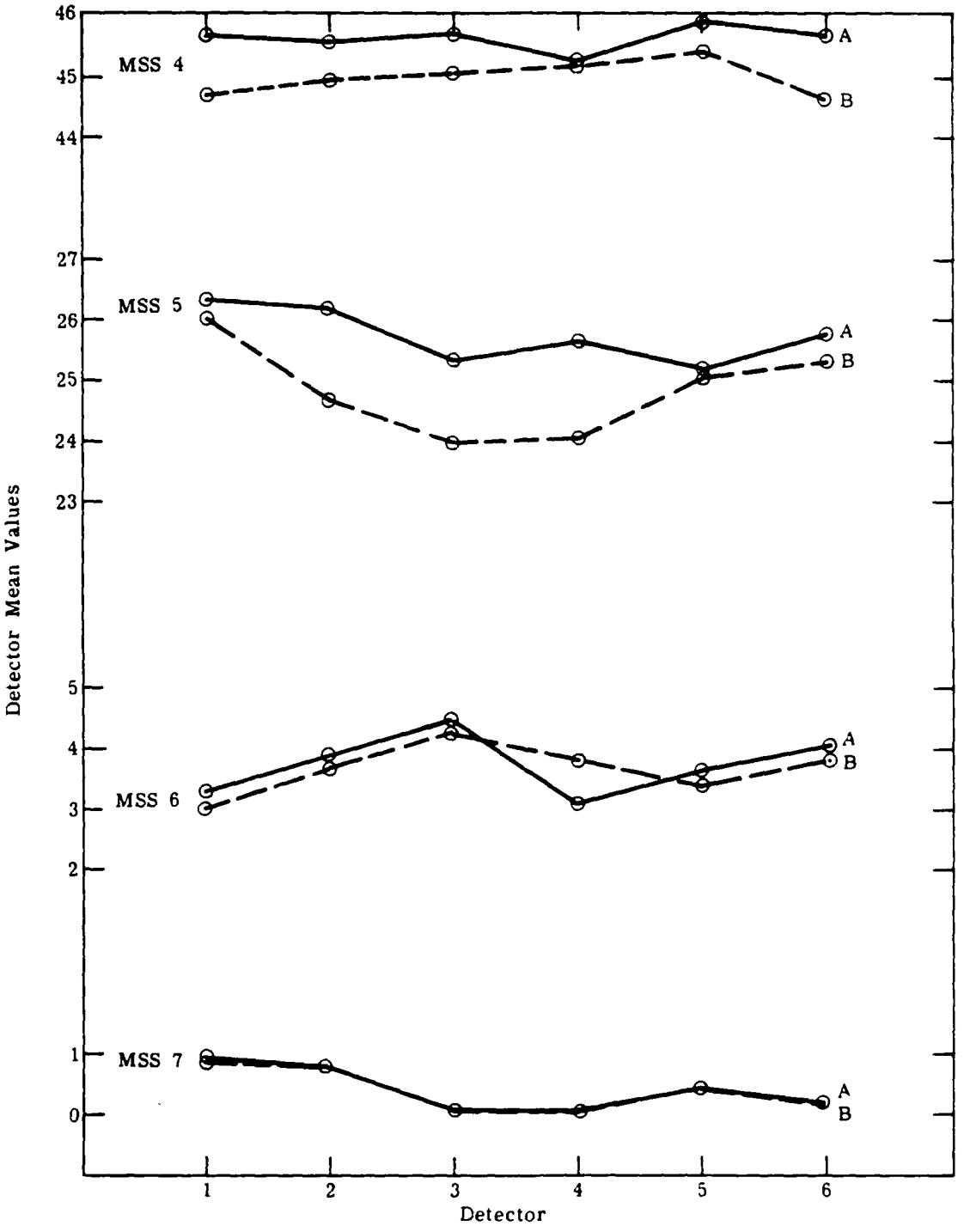

FIGURE 1. DETECTOR MEAN VALUES OVER OPEN WATER FOR TWO AREAS IN LANDSAT FRAME 11249-14435, STRIP 3. Area A: Lines 325-354, Points 1-200. Area B: Lines 1045-1074, Points 1-200.

acceptable limits, or a line-by-line correction must be made. The former procedure can be used with any destriping algorithm, subject to the constraints discussed in the previous paragraph, while a line-by-line correction can be reliably done only with the offset algorithm because the parameters required for the other algorithms cannot be reliably obtained from a single line of data.

A more detailed discussion of each type of correction algorithm is presented in the following subsections.

2.1 OFFSET CORRECTION

The first step in obtaining the offset correction parameters is to compute the mean signal values for each detector (i.e., each sixth line) over a selected area. This area may include a range of signals, if each detector views the same distribution of radiances, but for hydrographic applications the best results are obtained if an area of clear deep water is selected. The rationale for this selection is three-fold: first, since such an area presents a uniform radiance, the requirement of equal radiance distributions for all detectors is easily met even for relatively small areas. Second, since the simple offset correction guarantees removal of detector differences only for a limited range of signals, the selection of a deep water area insures that an optimal correction will be obtained for signals near the deep-water signal, where the depth extraction algorithms are most sensitive to noise. In terms of the depth error incurred, a detector-to-detector variation of several counts near the upper limit of the signal range may have less effect than a variation of one count near the deep-water signal. The third reason for the selection of a deep water area for calculating striping coefficients is that the deep water signals are needed for subsequent depth processing, so the collection of statistics for deep water serves a double purpose.

After the detector mean values have been obtained, a set of offset corrections (c_i) is determined. The criterion for an optimum correction

is that the variance among detectors is minimized. This variance is defined by

$$\sigma^2 = \frac{1}{6} \sum_{i=1}^{6} (V_i + C_i - \bar{V})^2$$

where

$$\bar{V} = \frac{1}{6} \sum_{i=1}^{6} (V_i + C_i)$$

and V_i is the mean value for detector i and C_i is the offset correction factor for detector i. If real arithmetic is allowed, the optimum correction factors are given by

$$C_i = \bar{V} - V_i$$

and the variance can be reduced to zero. However, if the corrected data is to be stored in the same integer form as the raw data, only integer-correction factors are allowed. In this case, it can be shown that merely rounding off C_i to the nearest integer value is not necessarily the optimal solution [1], but that the optimal solution can be obtained by adding n/6 to C_i before rounding off, where n is an integer from 1 to 6. Since the actual value of n which results in the optimal correction cannot be predicted a priori, each of these six possible sets of correction factors must be generated and tested to find the optimal one.

2.2 OFFSET AND GAIN CORRECTION

Two methods have been developed for making simultaneous corrections for both offset and gain differences among detectors. The first method requires that detector mean values be calculated for two (or more) areas, each of which has a different average signal, and within which the signals are uniform or slowly varying. If $V_i(A)$ is the

mean value for detector i in area A, V(A) is the "correct" value (e.g., the average overall detectors), and $V_i(B)$ and V(B) are the corresponding values for area B, then the corrected signal for detector i can be written as

$$V'_i = V(A) + \frac{V(B) - V(A)}{V_i(B) - V_i(A)} [V_i - V_i(A)]$$

where V_i is the uncorrected signal [2]. This correction assumes that the detector responses are colinear. If there are nonlinearities, the procedure can be adapted by using the average signals in three or more areas and approximating the non-linear curve by a piecewise linear function.

The second method of obtaining the parameters for a linear or piecewise linear correction of detector-to-detector variations is to do a least-squares fit or a linear regression between the signals for one detector and the signals for each of the other detectors in turn. This procedure requires the assumption that the data set can be decomposed into a set of N signal pairs (V_{in}, V_{jn}), n = 1...N, where V_{in} is the signal for detector i and V_{jn} is the signal for detector j, such that these signals correspond to the same radiance. (The most natural way to form these pairs is to use signals from the same point number on the same mirror sweep.) This assumption will be approximately valid if the frequency of spatial variations is small compared with the sampling rate. This condition is met in some oceanic scenes, such as those containing a gently sloping bottom with a uniform bottom reflectance, but not in all scenes. Thus, the scene must be carefully evaluated before applying this method.

Assuming that the conditions required for the application of this method are met, the correction coefficients are given by

$$a_i = \frac{\sum_{n=1}^{N} (V_{in} - \bar{V}_i)(V_{jn} - \bar{V}_j)}{\sum_{n=1}^{N} (V_{in} - \bar{V}_i)^2}$$

$$b_i = \bar{V}_j - a_i \bar{V}_i$$

where $\bar{V}_i = \frac{1}{N} \sum_{n=1}^{N} V_{in}$

and

$$\bar{V}_j = \frac{1}{N} \sum_{n=1}^{N} V_{jn}$$

This procedure effectively normalizes each detector i to a common detector j, assuming a linear relationship exists between the two detectors. If the relationship is non-linear, a piecewise linear fit may be obtained by partitioning the data set into two or more signal ranges and doing a separate least-squares fit for each range.

2.3 HISTOGRAM EQUALIZATION CORRECTION

The final type of destriping algorithm considered is the histogram equalization method described by Rosenberg [3]. In this method, cumulative histograms of data values are generated separately for each detector, and each original data value is reassigned a new value (via a lookup table) in order to force the histograms for each detector to be the same. Specifically, the procedure is to find, by interpolation, the signal values (V'_{in}) for each detector (i) corresponding to a cumulative frequency of n percent (n = 0, 1,..., 100). These values are then averaged over all detectors to give a set of "correct" signal values (V'_n) corresponding to the input values V'_{in}). However, since

these are in general non-integer values, a second interpolation is required to find the "correct" output values V_k corresponding to the integer input values V_{ik} for each detector.

The basic assumption involved in this algorithm is that each of the six detectors views the same distribution of radiances in the calibration scene. This is a somewhat less stringent requirement than those for the other algorithms described above. However, this condition must be met for the entire range of signals to be corrected, since the correction is valid only over the range of signals encountered the calibration scene. In the example cited previously of a scene containing large expanses of open water with only a few reefs or shoals, the conditions required for the application of this method would probably not be met since the upper range of signals would not be equally represented in all detectors. The primary advantage of this method, assuming that the required conditions are met, is that corrections can be made for highly non-linear deviations such as those introduced by the NASA signal decompression routine.

3
TASK 2 - RADIOMETRIC AND GEOMETRIC PROCESSING PARAMETERS

This section contains a description of the procedure used by NASA for processing Landsat data and preparing computer compatible tapes (CCTs). The information presented here was gathered from various sources, including the Landsat Data Users Handbook [4], NASA Landsat Newsletters and Bulletins, other NASA reports [5,6], and personal communications with NASA personnel. The descriptions are not intended to be complete or exhaustive, but focus on the aspects of the processing which are most crucial for hydrographic applications. Subsection 3.1 deals with the Image Processing Facility (IPF) used for processing Landsat-1 and Landsat-2 data, and subsection 3.2 describes the modifications to the IPF planned for handling Landsat-3 data. In subsections 3.3 and 3.4, recommendations are made for additional or alternative procedures for processing Landsat data intended for hydrographic applications.

3.1 LANDSAT IMAGE PROCESSING FACILITY

Data from Landsat is received at one of three NASA receiving stations and recorded on magnetic tapes which are brought to NASA/GSFC for processing and distribution. Processing is done on the Image Processing Facility (IPF) which converts the data to film imagery and also copies the data for selected scenes onto computer compatible tapes (CCTs). The subsystems which generate film imagery and CCTs are functionally separate and operate independently on the raw data received from the satellite. The Initial Image Generation Subsystem (IIGS), which produces the film imagery, applies its own set of radiometric and geometric corrections to the data based on internal calibration and orbital/platform parameters. The subsystems which produce CCTs apply a radiometric correction but no geometric corrections except for some re-ordering of the data to compensate for misregistration among spectral

bands and variations in scan line length. Since the process by which CCTs are generated is of primary interest, this process will be described in more detail in the following paragraphs.

Two stages are involved in the process of generating CCTs from the raw Landsat Multispectral Scanner data. The first stage is carried out by the Multispectral Scanner Preprocessor (MPP), which basically reformats selected portions of the raw video and calibration data onto high density tapes (HDTs). The second stage is performed by the Digital Subsystem (DS), which reads the high density tapes from the MPP as well as image annotation tapes containing orbit and platform data, makes radiometric corrections to the data and writes out the modified data on computer compatible tapes (CCTs).

In addition to the radiometric corrections, which will be described in the following paragraphs, two other operations are carried out by the DS on the raw video data. The first of these is the insertion of registration fill characters at the ends of each scan line in order to compensate for the band misregistration in the raw data caused by sequential sampling of the detectors. Because of the delay in sampling (combined with the displacement inherent in the 4 x 6 fiber optic matrix), the first pixel in MSS4 corresponds spatially to the third pixel in MSS5, the fifth pixel in MSS6, and the seventh pixel in MSS7. Therefore, in order to bring the bands into registration on the CCTs, six "fill characters" are inserted at the beginning of each line in MSS4, four are inserted in MSS5, and two in MSS6. This pattern is reversed at the end of each line in order to maintain the same line length for each band. The second operation carried out by the DS is a line length adjustment to compensate for variations in the number of samples per scan line from scene to scene. This adjustment is made by repeating pixels at regular intervals in each line. Because of the data format used for CCTs, the number of pixels in each output line must be a multiple of 24. The number of original samples per scan line is typically 3216 $\pm$ 16 for Landsat-1 and 3247 $\pm$ 5 for Landsat-2. After

adding the six registration fill characters, the maximum number of pixels is 3228 for Landsat-1 and 3258 for Landsat-2. Thus, the corrected line length is 3240 for Landsat-1 and 3264 for Landsat-2, and there are typically 18 $\pm$ 6 repeated pixels in Landsat-1 data and 11 $\pm$ 5 repeated pixels in Landsat-2 data.

The radiometric corrections applied to MSS data by the Digital Subsystem are a decompression to linearize data which has been transmitted from the satellite in compressed mode, and a radiometric calibration to compensate for changes in detector response characteristics with respect to the prelaunch calibration and to equalize changes among the six detectors for each band. Decompression is done by a table look up routine which reads in values from 0 to 63 and writes out values from 0 to 124. Except for input values of 2 and 3, which are both assigned on output value of 2, this transformation is single-valued. However, since only 63 output values are assigned, there are "gaps" of one or two counts in the output signal which may contribute to the striping problem by accentuating differences among the detectors.

The radiometric calibration is done separately for each detector and each scan line, using the calibration data which is recorded at the end of each mirror scan. This calibration data is obtained by viewing an internal light source through a varible neutral density filter during the retrace interval. Initially, about 900 samples are recorded across the calibration wedge, but a subset of six of these samples are selected by the MPP and copied onto the HDTs for further processing. (On Landsat-1, only four useable samples were selected in high-gain mode, since the first two were saturated.) During preflight calibration tests, the signal values from these calibration samples were compared with signals obtained by scanning across an external standard radiance source, and a set of regression equations were obtained relating the gain coefficient (b) and the offset coefficient (a) to the calibration signals for each detector and each band. Thus in principle it is possible to calibrate each scan line individually, using the calibration

signals for that scan line to calculate $\hat{a}$ and $\hat{b}$, and modifying the data using the equation

$$V'_i = \frac{1}{\hat{b}_i} [V_i - \hat{a}_i]$$

where V_i is the raw data value (after decompression) in detector i. In practice, because of noise in the calibration signals, a modification of this procedure is used in which the values $\hat{a}_i$ and $\hat{b}_i$ are "filtered" or averaged over a number of scan lines before being used for averaging.

The radiometric calibration process used for Landsat has encountered two unforeseen difficulties. First, the process has not completely succeeded in eliminating calibration differences among the six detectors. As a result of this partial failure, a modification of the algorithm was developed and has been implemented as of July 6, 1977. In the new algorithm, the data is first calibrated using the procedure described above, and then a second offset and gain correction is made using correction factors which are constant over each full frame of data. The correction factors are derived from an analysis of Landsat data over a period of time, by a procedure which has not yet been published by NASA. The second difficulty was revealed by an analysis of variations in the calibration data. The calibration signal should be independent of the external scene viewed by the satellite, but it has in fact been found to be correlated with the average scene brightness. The reason for this correlation has not been conclusively determined, but it is thought to be due to a hysteresis or memory effect in the photomultiplier detectors. The implication of this finding is that the calibration of the data is suspect in areas where there are large variations in scene brightness, for example in oceanic areas partially covered with clouds. This effect, combined with the line-by-line calibration procedure, may also contribute to variations in the striping pattern as discussed in section 2 of this report.

3.2 MODIFICATIONS OF THE IPF FOR LANDSAT-3

Several major modifications are being implemented in the Image Processing Facility for handling Landsat-3 data (current estimates are for the new system to be operational by the beginning of 1979). Perhaps the most significant change for the present application is that geometric corrections as well as radiometric corrections will routinely be made before generation of the CCTs. The standard mode for the geometric corrections will be cubic convolution, although nearest-neighbor resampling will be available as an option. There are plans to make these corrections using ground control points for U.S. images, although these will probably not be available for the first year of operation. Until the ground control point library is completed, and for most-foreign scenes, the geometric corrections will be made using satellite orbital and attitude parameters. Data will be resampled onto a square 57 x 57 meter grid and copied onto HDTs at NASA/Goddard. These HDTs will be sent to EROS Data Center for conversion into CCTs and film products for distribution to the user community.

3.3 RECOMMENDATIONS FOR RADIOMETRIC CORRECTIONS

It has become apparent that while the standard method of processing Landsat data at NASA/Goddard may be acceptable for most terrestrial applications, a more specialized processing procedure would be of benefit for hydrographic applications of Landsat data. These applications require that a maximum amount of both radiometric and geometric information be preserved during processing, even at the cost of increased data processing complexity on the part of the user. In this subsection, recommendations are made for alternative radiometric processing methods for Landsat data. Geometric processing is described in the following subsection. Since these procedures are presumed to be carried out on raw data, their implementation would require that this data be obtained directly from NASA without going through the regular

processing channels, or that special provision be made to disable some of the routine processing steps and a special uncorrected product made available to hydrographic users.

The primary disadvantage of the NASA radiometric correction algorithm is that the outputs from both correction steps (decompression and calibration) are transmitted in integer mode, and are, therefore, subject to roundoff errors which might be significant for hydrographic applications. If line-by-line radiometric corrections are considered to be a necessity, it is probably inevitable that at least the final output be converted into integer form for recording on magnetic tape. However, it is not clear that the decompression output needs to be in integer form, since this output is immediately used in the radiometric calibration process, which uses floating-point arithmetic. It is also not clear that a line-by-line radiometric calibration is superior to a full frame calibration*. If full frame calibration is used, it would be possible to copy the raw data directly to CCTs and supply users with a 24 x 64 element look-up table in floating point form which would allows users to make a full radiometric correction (decompression and detector calibration) without incurring any further roundoff errors.

If it can be demonstrated that a line-by-line calibration is necessary it is recommended that a modified calibration procedure be used on tapes intended for hydrographic applications. This procedure would eliminate the filtering or smoothing of calibration data and use only the calibration data for a given scan line to calibrate that scan line. To reduce noise, all available calibration data (900 samples) except

*Full frame calibration is done, for example, by the Canadian processing facility. A test is being planned to compare the results of the two processing methods on a common data set, preferably one with large variations in average brightness.

that which is saturated in high-gain mode would be used for calibration instead of the six samples currently used. This would probably be prohibitively expensive for routine processing, but could be done on a limited number of scenes. If this were done by an external agency such as DMA, it would require access to the raw video tapes, since even the intermediate HDTs contain only a subset of six calibration samples. It is also recommended that after calibration, the data be recorded using all 8 bits per byte instead of 7 as is currently done. The only reason for reserving one bit as a flag is apparently to indicate registration fill characters, but since these always occur in the same locations it does not seem necessary to flag them.

If the advantages of line-by-line calibration cannot be demonstrated, it is recommended that full-frame calibration be implemented using the look-up table method described above. If NASA is unwilling to make such a change, it is recommended that DMA seek access to raw (uncorrected) data tapes and perform their own full-frame calibration by averaging the calibration data over the entire scene, and perhaps also by obtaining statistics from the video data as outlined in section 2 of this report.

3.4 RECOMMENDATIONS FOR GEOMETRIC CORRECTIONS

Since geometric corrections are not currently done before CCT generation, these corrections may be applied by the user to the CCTs as received (although the first step in this process should be the removal of the repeated pixels inserted by NASA to equalize line lengths). Several software packages for making geometric corrections to Landsat data are already in the public domain including the Digital Image Rectification System (DIRS) developed by the Information Extraction Division at NASA/Goddard [6]. Resampling for the purpose of making geometric corrections can be done by several methods, including nearest-neighbor and cubic convolution methods. Studies [7,8] have shown that

while cubic convolution enhances the appearance of the image and is able to correct for subpixel discontinuities, it has considerable disadvantages for the present application. These disadvantages are that high spatial frequencies are attenuated, small features are distorted by "overshoot" and spreading, and data values are altered in a manner which is highly dependent on the sampling lattice. The nearest-neighbor method, although it cannot make corrections to less than one-half pixel accuracy, preserves all of the original data values and has essentially no effect on spatial frequencies. The nearest-neighbor method is also the only method which can be applied to data which has been classified or processed in such a manner that output data values are not linearly related to radiance. Our recommendation is, therefore, that data processing should be carried out as far as possible on uncorrected data, and that resampling should be done by the nearest-neighbor method only when necessary for purposes of display or registration with other data sources. It should also be noted that much of the resampling for display purposes can be eliminated by special design of the display equipment (e.g., non-square picture elements).

The new NASA IPF being built for Landsat-3 data poses some problems for hydrographic users, since the standard mode of operation will be to resample the data by a cubic convolution method onto a square 57 x 57 meter grid. The option to use nearest-neighbor resampling will exist, and would probably be the more desirable of the two alternatives, but either method will almost certainly degrade the useability of the data for hydrographic applications and make corrections for detector-to-detector variations more difficult to accomplish. Our recommendation is, therefore, again for DMA to seek access to raw (uncorrected) data tapes and carry out their own geometric corrections when necessary. This is especially true for foreign scenes for which NASA will not have ground control points. Rather than do a second geometric correction using ground control points specifically acquired by DMA for this purpose, it would be more advisable to carry out these corrections only once, and when necessary, on the raw data.

4
TASK 3 - MULTITEMPORAL PROCESSING METHODS

One of the principal advantages of Landsat as a source of data for hydrographic mapping is its repetitive coverage of a given scene at 18 day intervals. This repetition not only permits the identification and separation of permanent features from transient effects, such as water quality and atmospheric variations, but also may be used to reduce dependence on surface measurements by allowing the extraction of water attenuation parameters from an analysis of scenes at different tidal stages. The methods and procedures which have been developed for such multitemporal analyses are described in this section. The application of these methods to actual data is described in section 6 of this report.

4.1 MULTITEMPORAL SCENE REGISTRATION

The first stage in a multitemporal processing sequence is the preparation of a composite data set in which corresponding pixels from each separate data set are brought into registration with each other. This registration can be done directly or through dual rectification. Direct registration involves a superposition of one data set onto another in a single step, while dual rectification involves a resampling of both data sets onto a common grid. Since each resampling process incurs some error or loss of information, the direct registration method is generally to be preferred. This method is also more computationally efficient and easier to apply, since only relative control information is needed, and this information can be obtained in a semi-automatic process from the data itself.

In order to superimpose one data set on another, a set of transformation equations must first be defined which relate the coordinates of one data set to the other. Several forms may be used for this transformation, including linear, piecewise linear (affine) and polynominal equations. The linear and affine transformations are of the form

$$L_2 = a_0 + a_1 L_1 + a_2 P_1$$

$$P_2 = b_0 + b_1 L_1 + b_2 P_1$$

where L_1, P_1 are the coordinates (line and point numbers) for the first data set and L_2,P_2 are the coordinates for the second data set. In the linear transformation, the constants in these equations are obtained by doing a least squares fit over the entire set of ground control points for the scene, and the resulting equations are assumed to be valid for the entire scene. In the affine transformation, the scene is subdivided into a set of triangles by drawing lines between the ground control points, and a separate set of equations is used for each triangular region. The constants in each set of equations are obtained by requiring an exact fit at each vertex (i.e., a linear interpolation is done between the nearest three ground control points). In the polynominal transformation a least-squares fit is done for the entire scene, as in the linear case, but terms of order higher than one are included in the equations.

In the registration procedure which has been developed during this contract, a linear transformation is used for the following reasons. In most coastal and oceanic scenes, the selection of ground control points is limited to a relatively small number of coastal features, islands, etc. Furthermore, there is often the possibility of a shift in these features due to tidal state or erosion/deposition. Therefore, it is felt that a more accurate overall transformation can be obtained by a least-squares fit which does not rely too heavily on any single control point, but uses a "concensus" among all available points. This rules out the affine transformation, which could introduce errors in the vicinity of a bad control point. The linear transformation is preferred over the polynomial because the number of control points is generally not large enough to accurately determine the higher-order terms, and the inclusion of these terms can cause large errors when extrapolating

beyond the region bounded by the control points. In the data sets which have been processed so far, no significant nonlinearities have been observed which would warrant the inclusion of higher order terms in the transformation equations.

Control points are obtained by locating common features in both data sets and recording the coordinates of these features. This may be done manually, by inspection of graymaps or other displays of the data, or it may be done using a semi-automatic method. In this method, the two-dimensional cross-correlation function is computed for the two data sets in the vicinity of each control point. The correlation function is assumed to be maximized when the control points are properly aligned. Thus, a point is chosen in one data set and an automatic search can be made to locate the corresponding point in the other data set. In practice this search is restricted, in order to save computer time, by indicating the approximate location of the control point in the second scene. The amount of user interaction in the form of selection of points and evaluation of results is desirable.

Once control points have been obtained and regressions have been run to determine the coordinate transformation equations, the data from the second scene are resampled and merged with the first data set. This is currently done by the nearest-neighbor method, rather than by interpolation, for the reasons outlined in section 3.4 above. Thus, for each pixel in the master data set, the corresponding coordinates are calculated for the second data set, the pixel nearest to this location is selected, and the two corresponding pixels are combined and written out on the output file. For two Landsat scenes with four bands or channels each, the output file would contain eight channels of data: the first four being the four bands of the master data set and the last four from the second data set.

A modification of this procedure may be used for registration of data from different sources, such as aircraft scanner data or digitized film imagery. This modification is to first resample the data set

having the coarser spatial resolution onto a grid with the same resolution and orientation as the finer data set. Then, the correlation function technique described above is used to align the data sets in the vicinity of each control point. Finally, the second data set is resampled and merged with the master data set. If the master data set is the one with the coarser spatial resolution, and the resolution difference is such that two or more of the smaller pixels are contained within the larger ones, the registration procedure should average all of these pixels together rather than pick the single pixel closest to the center of the master data set pixel.

4.2 IDENTIFICATION AND SEPARATION OF TRANSIENT EFFECTS

After two or more Landsat data sets have been spatially registered, several types of multitemporal processing techniques can be applied. These include temporal averaging, change detection, and removal of transient effects. The simplest type of processing is temporal averaging, in which the data sets are averaged together on a pixel-by-pixel basis in order to reduce random noise in the data. Because of the exponential dependence of the signal on the water depth, as explained in section 4.3, this averaging must be done in a special way to preserve the form of this relationship. A simple arithmetic average of the signals from two or more scene dates would no longer be exponentially related to depth except in the cases where the water attenuation parameters and the solar elevation is the same for each overpass. In the general case, the exponential relationship can be preserved by taking the product of each corresponding data value after subtracting the mean deep water signal. Alternatively, the exponential relationship can be transformed into a linear one by taking the logarithm of the signal after the deep-water subtraction. Subsequent to this transformation the data may be scaled to remove differences in water attenuation and sun elevation, and arithmetically averaged in the usual way.

Random noise is characterized by a lack of spatial coherence in the observed signal differences between multitemporal data sets. This coherence or lack of coherence can probably best be judged by inspection of a map or display of the signal difference after a logarithmic transformation and scaling as described in the preceeding paragraph. Where a consistent spatial pattern appears in such a display, a different type of processing other than temporal averaging is called for. If the goal of the processing is to detect long-term changes, for example topographic changes due to erosion or deposition, the difference map itself may represent the final product. If, on the other hand, the purpose of the processing is to eliminate transient effects such as water turbidity or atmospheric variations, a third type of processing is necessary. In this transient removal algorithm, the data values from each data set are compared, a decision is made as to the "correct" data value at a given location, and this data value is transferred into the output file.

Actually several types of transient removal algorithms are conceivable. For the case of the bitemporal data set (comprised of two temporal acquisitions), the simplest algorithm would merely select the lower of the two values on the assumption that most transient effects (increased water turbidity, atmospheric haze, etc.) cause an increase in the observed signal. This algorithm selects the wrong data value in the case of cloud shadows or strongly absorbing materials in the water, however. Another possibility would be to choose the value nearest to the preceding data value, although this procedure could also give incorrect results in some cases. Both of these procedures could be improved by applying a difference criterion to determine whether the changes are due to random noise or transient effects. For example, the rms difference between the entire data sets could be determined during a screening pass through the data. During processing the difference between each individual pair of data values are then compared with this rms difference. If the difference is below the threshold, the data values are averaged together to improve the signal-to-noise ratio, but if

the difference is larger than the threshold the "correct" value is selected by one of the above-mentioned criteria.

If three or more temporal data sets are used, a somewhat more reliable transient removal can be effected by a "voting" procedure. In this case, the central value could be selected, or the central value and the value nearest the central value could be averaged together, or the set of values which differ by less than a given threshold could be averaged together. Any of these algorithms would give more accurate results than is possible for the bi-temporal case, since it is unlikely that two samples would be affected by transients at the same location.

4.3 EXPLOITATION OF TIDAL DIFFERENCES FOR WATER PARAMETER EXTRACTION

Differences in tidal state between two data sets covering the same geographical area may be used to extract some information about water parameters if these parameters and the sun elevation are the same for both dates. For this purpose the data sets need not be actually registered, but the relationship between the coordinates of the two data sets must be known. The procedure is to select areas containing deep water (where no bottom return is present) and shallow water (where a strong bottom return exists). Corresponding areas are selected in both data sets, and mean signal values are computed for each area. The difference between the mean shallow water signal and the mean deep water signal is denoted by $\overline{\Delta V_1}$ and $\overline{\Delta V_2}$ for data sets 1 and 2, respectively. Assuming that the tidal state is known for both data sets, and that the sun elevation and water optical properties are the same for both data sets, some information about the water optical properties may be inferred from the relative magnitudes of $\overline{\Delta V_1}$ and $\overline{\Delta V_2}$. This inference is made on the basis of the following argument.

The signal recorded by Landsat over shallow water may be written approximately as:

$$V = V_d + ar_b e^{-(1 + \sec \theta')Kz}$$

where V_d is the deep water signal, a is a parameter depending on the atmospheric state and the solar irradiance, r_b is the bottom reflectance, θ' is the apparent solar zenith angle underwater, K is the effective water attenuation coefficient, and z is the water depth. For the first overpass, we may, therefore, write

$$\overline{\Delta V_1} = a_1 \left\langle r_b e^{-(1 + \sec \theta'_1)Kz} \right\rangle$$

where the brackets indicate an average value over the shallow water scene. For the second overpass, each point in the scene has a water depth $z + \Delta z$, where Δz is the difference in tidal height between the two overpasses. Thus, the average signal difference for the second data set may be written as

$$\overline{\Delta V_2} = a_2 \left\langle r_b e^{-(1 + \sec \theta'_2)K(z + \Delta z)} \right\rangle$$

Measurements of $\overline{\Delta V_1}$ and $\overline{\Delta V_2}$ can be used to extract the value of K without detailed knowledge of the depth in the scene if the sun angles are the same for both overpasses. If the sun angles are not the same, K values cannot be extracted without knowledge of z and there is no particular advantage in the multitemporal approach.

For the case of two data sets with the same sun angle ($\theta'_1 = \theta'_2$) we may write

$$\frac{\overline{\Delta V_1}}{\overline{\Delta V_2}} = \frac{a_1}{a_2} e^{K(1 + \sec \theta')\Delta z}$$

or

$$K = \frac{\ln\left(\frac{\overline{\Delta V_1}}{\overline{\Delta V_2}}\right) - \ln\left(\frac{a_1}{a_2}\right)}{(1 + \sec\theta')\Delta z}$$

The value of $\frac{a_1}{b_1}$ will differ from 1 only if the atmospheric state is different for the two overpasses -- for most cases this difference may be neglected and the term involving $\frac{a_1}{b_1}$ may be dropped from the equation. An evaluation of the atmospheric state can be made by comparing the signal difference for two targets (e.g., beach sand and deep water) in both data sets. If the signal difference is not the same for both overpasses, the value

$$\frac{a_1}{b_1} = \frac{V_{b1} - V_{d1}}{V_{b2} - V_{d2}}$$

should be used in the equation for K, where V_{b1} is the signal over a bright object in data set 1, V_{d1} is the signal over a dark object, etc.

4.4 MULTITEMPORAL DEPTH EXTRACTION TECHNIQUES

Assuming that the data has been logarithmically transformed as described in section 4.2, and either temporally averaged or edited to remove transient effects, the resultant data values may be expressed as

$$X = \ln(ar_b) - (1 + \sec\theta')Kz$$

The constants in this equation may be determined by measurements of r_b and K or by measurements of z at several locations. If the bottom reflectance is uniform in the scene, this equation can be simply inverted to yield the depth at each point. If the bottom reflectance is variable, a correction can be made for these variations if the depth is shallow enough so that a bottom-reflected signal is recorded in MSS5.

The simplest such correction assumes a uniform reflectance ratio in MSS4 and MSS5. Thus, the depth is given by

$$z = \frac{X_5 - X_4}{(1 + \sec \theta') (K_5 - K_4)}$$

A more general correction for bottom color corrections can be made by using more complicated functions of X_4 and X_5 [9].

5
TASK 4 - ATMOSPHERIC AND SURFACE REFLECTION EFFECTS

A preliminary survey has been made of existing techniques for separating the contributions of atmospheric scattering and surface reflectance from the subsurface reflectance of the ocean. This task will continue into the next year with the examination of various Landsat scenes under different illumination conditions.

Basically, there are two methods of extracting information about atmospheric effects from multispectral scanner data in the visible and near-infrared regions of the spectrum. The first is the method of examining the discontinuities in radiances at the edges of shadows in the image. This method was originally formulated by Piech and Walker [10] as follows: the radiance of a given object with reflectance R is

$$L = \alpha R + \beta$$

in direct sunlight, and

$$L' = \alpha' R + \beta$$

in shadow, where α is proportional to the atmospheric transmittance and the total irradiance, α' is proportional to atmospheric transmittance and skylight irradiance, and β is the path radiance ("air light"). These two equations may be combined into the equation

$$L = \left(1 + \frac{\delta}{\alpha'}\right) L' - \frac{\delta}{\alpha'} \beta$$

where $\delta = \alpha - \alpha'$. Thus, by plotting L versus L' for at least two objects with different reflectances the slope $\left(1 + \frac{\delta}{\alpha'}\right)$ and intercept $\frac{\delta}{\alpha'} \beta$ may be determined, from which β and $\frac{\delta}{\alpha'}$ can be calculated. If the reflectance of one object is known, the absolute values of α and α' can also be determined.

This technique can be applied to ocean scenes if distinct cloud shadows exist over at least two regions of different reflectance (e.g., deep water and shallow water). It should be noted that the term β in this case is actually the sum of the path radiance and the surface-reflectance radiance. Since the surface reflects skylight more or less specularly, depending on the sea state, the surface-reflected radiance will be the same in direct sunlight and in the shadow (assuming that the view angles are such that the image of the cloud is not reflected into the field of view). This component is, therefore, included in the value of β determined by this method.

This method assumes that the reflectance R is the same for skylight and sunlight, which is not precisely true for ocean scenes but is probably accurate enough for the intended purpose. The technique is primarily useful for determining the ratio (δ/α') of direct illumination to diffuse illumination. Since volume scattering contributes a negligible amount to the radiance observed by satellite over the open ocean, the value of β is for all practical purposes the same as the deep-water signal, which can usually be observed directly.

The second method of extracting information about atmospheric effects is through an examination of the signal in the red or near-infrared region of the spectrum. At these wavelengths the water attenuation is so high that a negligible subsurface reflectance exists in moderately clear and deep water. Thus, the total radiance observed under these conditions is due to atmospheric scattering. By comparing this observed radiance with the radiance calculated from an atmospheric model, the optical thickness can be obtained. The model can then be used to calculate the path radiance and transmittance in the visible region in order to make corrections for atmospheric variations in the scene. Models and procedures have been proposed by several authors [11, 12, 13], and the concensus of opinion appears to be that MSS6 is the most useful band for extracting atmospheric parameters. These procedures will be evaluated during the next year, and an attempt will be made to develop a method of automatically correcting for atmospheric variations in oceanic scenes.

6

TASK 5 - MULTITEMPORAL PROCESSING OF BAHAMA DATA

The groundwork has been laid for multitemporal bathymetric processing of Landsat data, and plans have been made to process several data sets from orbit number 232 covering part of the Great Bahama Bank. However, because of delays in the delivery of these data sets, all of the anticipated processing has not been completed at the time of writing this report. Processing will continue as these tapes are received, and all products and reports of this processing will be delivered upon completion of this task.

In the interim, some multitemporal processing has been done for two frames of data for this area. The two frames selected for this preliminary study are a low gain data set collected on 29 December 1974 (frame 10889-15033) and a high gain data set collected on 24 December 1975 (frame 11249-14435). Because of the similarity in the dates the sun angle are nearly the same for both data sets. The first data set was taken about two hours after high tide, and the second was about two hours before high tide, so the tidal levels are nearly the same for the two data sets also.

The first step in the processing of these data sets was the extraction of relative control points and registration of the two scenes using the techniques described in section 4.1 of this report. The next step was a scaling of the low gain bands to make them commensurate with the high gain data. Figures 2-5 show plots of the low gain and high gain MSS-4 and MSS-5 data along two lines near North Cat Cay and South Cat Cay in the Bahamas. Figures 6 and 7 show two-dimensional histograms of data values in the low gain bands versus those in the high gain bands. A least-squares fit was done between the low and high gain data, resulting in the following equations:

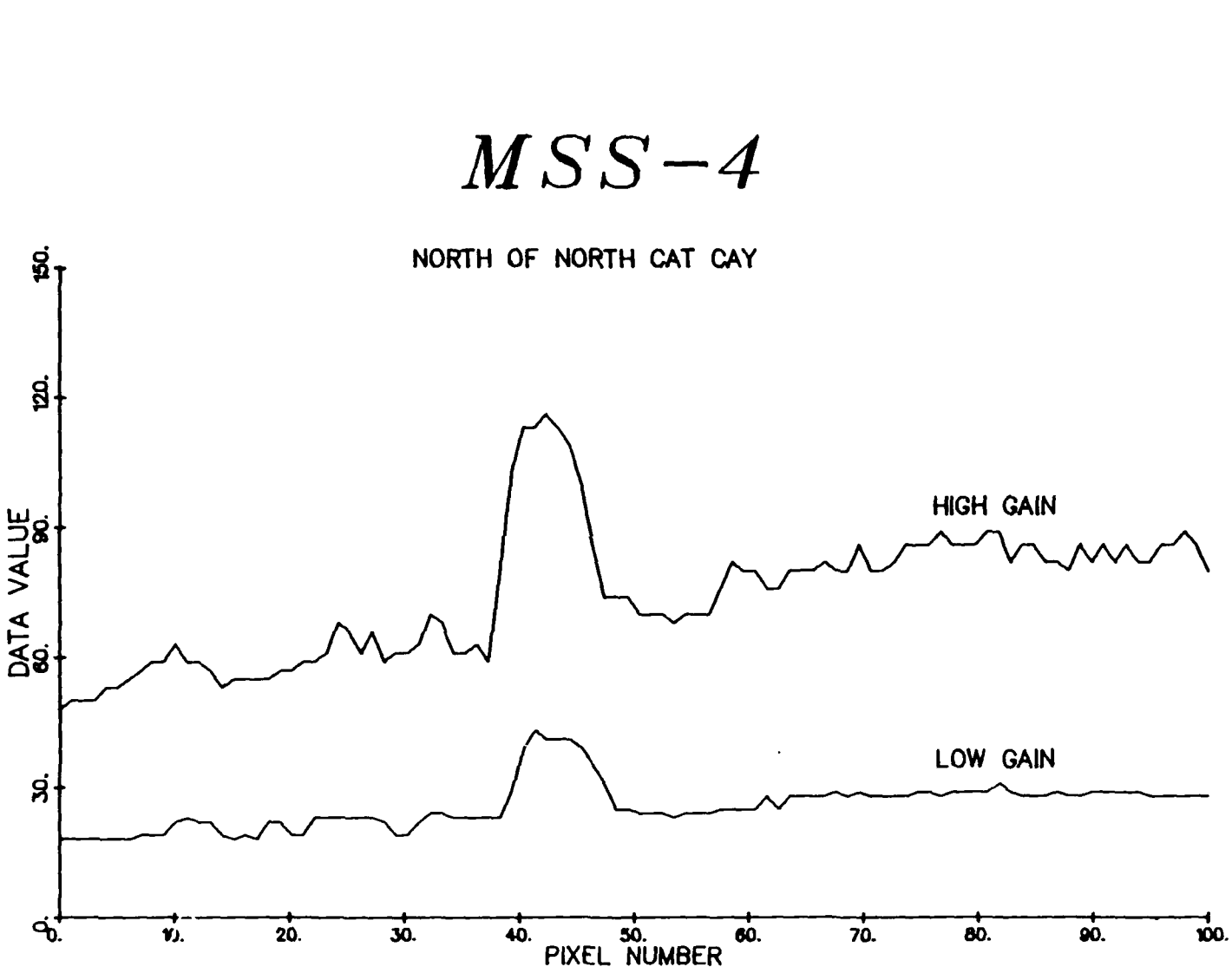

Figure 2. Plots of Raw Low Gain and High Gain MSS4 Data North of North Cat Cay, Great Bahama Bank

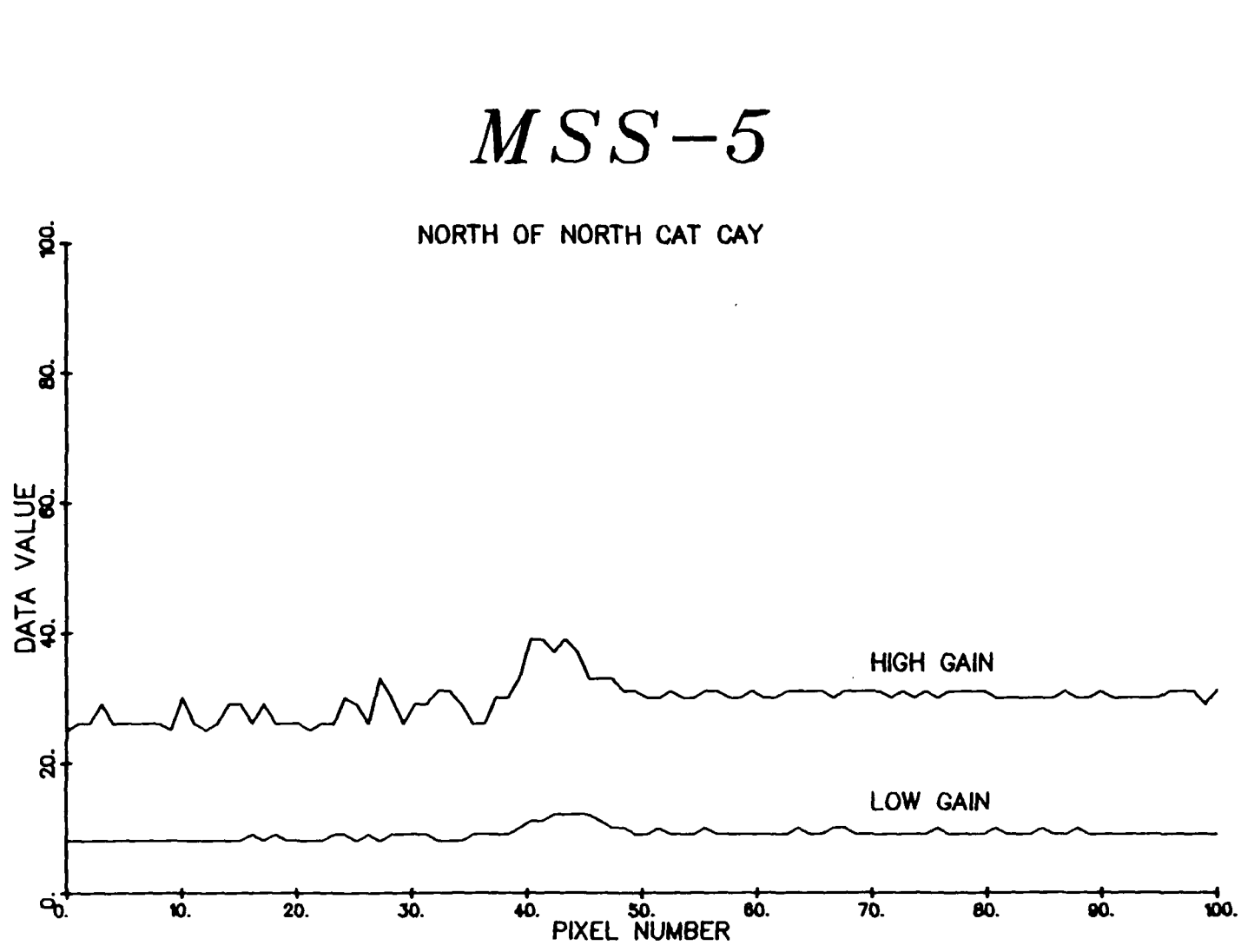

Figure 3. Plots of Raw Low Gain and High Gain MSS5 Data North of North Cat Cay, Great Bahama Bank

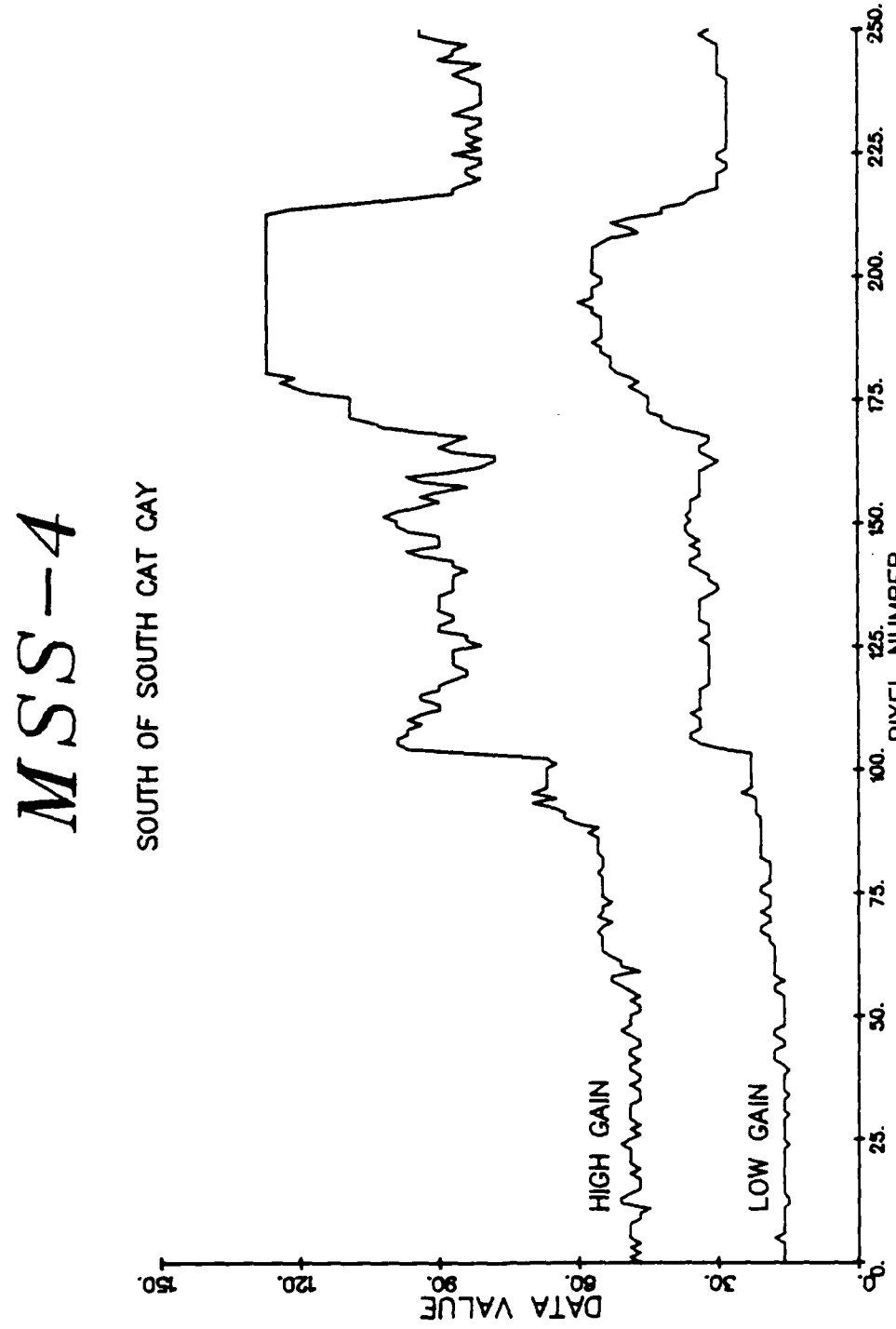

Figure 4. Plots of Raw Low Gain and High Gain MSS4 Data South of South Cat Cay, Great Bahama Bank

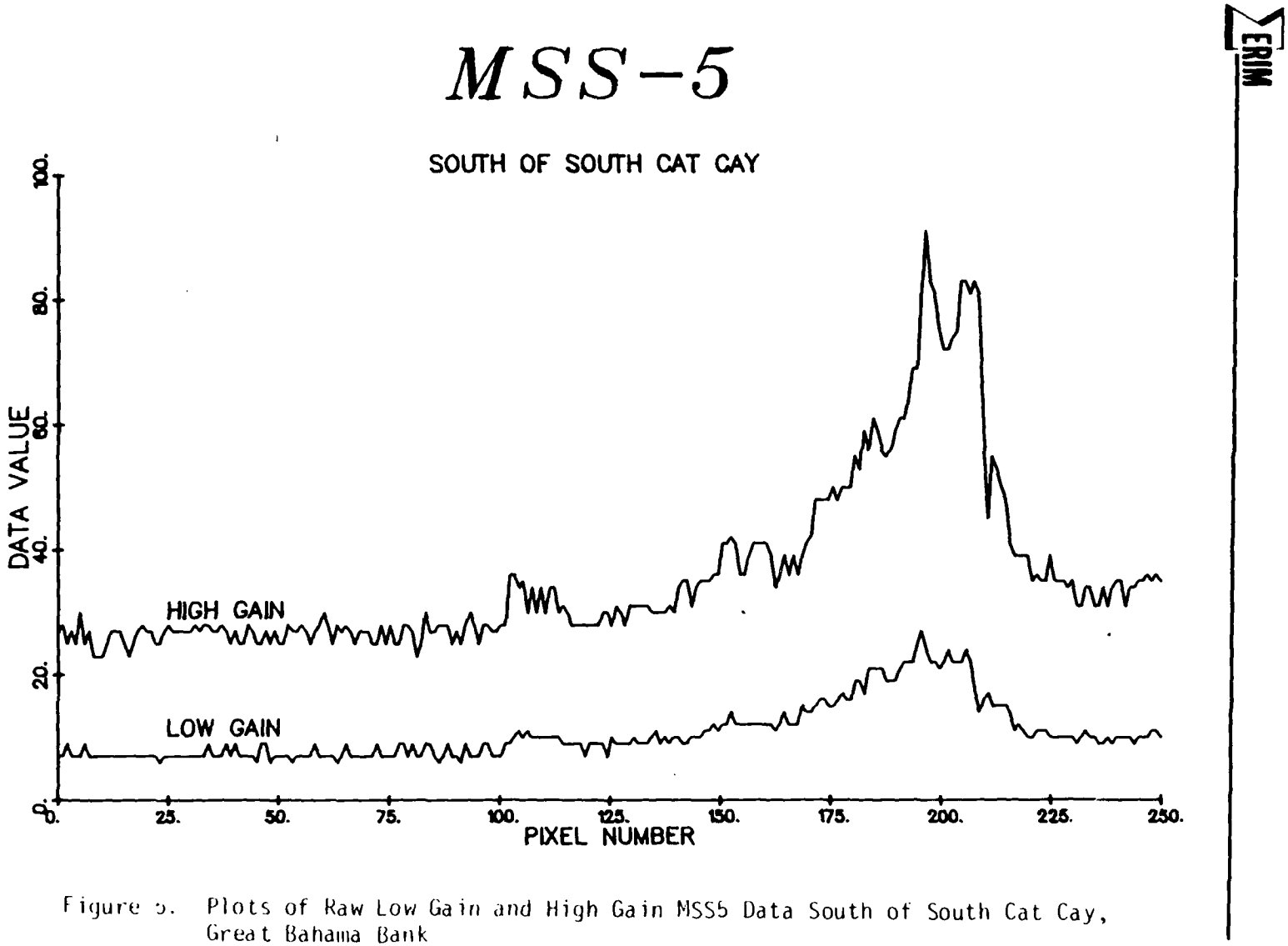

Figure 5. Plots of Raw Low Gain and High Gain MSS5 Data South of South Cat Cay, Great Bahama Bank

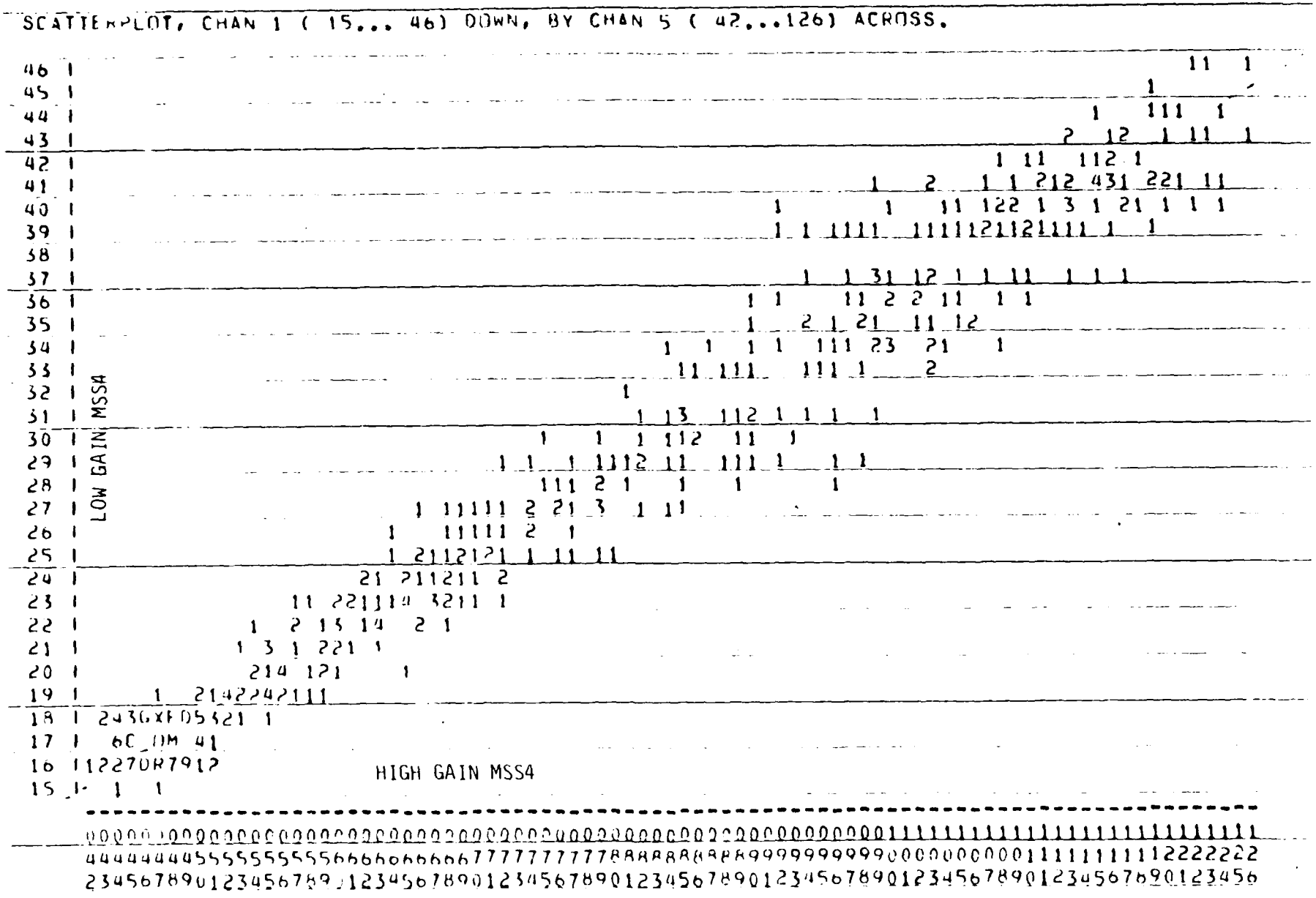

Figure 6. Correlation of Low Gain and High Gain MSS4 Data Values Near North Cat Cay, Great Bahama Bank

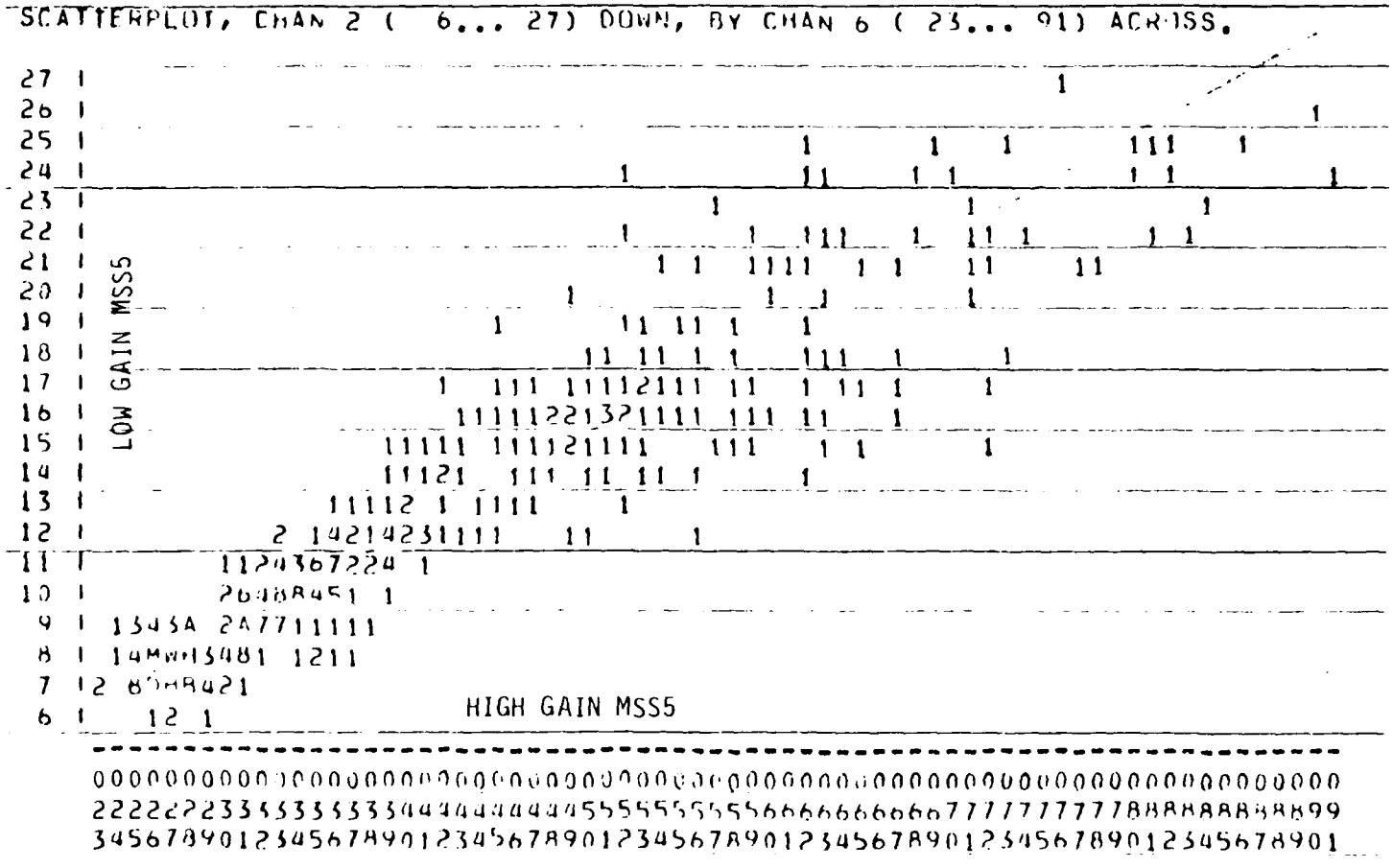

Figure 7. Correlation of Low Gain and High Gain MSS5 Data Values Near North Cat Cay, Great Bahama Bank

HIGH GAIN MSS 4 = 0.93 + 2.82 (LOW GAIN MSS 4)
HIGH GAIN MSS 5 = 3.46 + 3.30 (LOW GAIN MSS 5)

This analysis shows a considerable departure from the nominal 3x gain difference for MSS4. The standard deviation of the deep water signals was also calculated for the low gain and high gain bands. These figures, shown in Table 1, indicate that there is a slightly higher signal-to-noise ratio for the high gain data than the low gain data, by a factor of about 1.4 in both bands. The low gain data channels were scaled using the above equations, and the resulting data were again plotted along the same lines as in Figures 2-5, and are shown in Figures 8-11.

After registration and scaling, the two data sets were combined together using a transient suppression algorithm to remove clouds and whitings, and improve the signal-to-noise ratio of the data. This algorithm tests the difference between the data values in the two data sets on a pixel-by-pixel basis. If this difference is larger than a given threshold in MSS5, a cloud or whiting is assumed to be present and the data set having the lower data values is assumed to be the correct one. A test is also made to determine if the high gain data is saturated, and if so the low gain data is used. If no clouds or whitings are present in either data set, and the high gain data is not saturated, the data values from both data sets are averaged together to reduce the random noise in the data.

The results of the multitemporal transient suppression algorithm are shown in Figures 12 and 13. Figure 12 shows the raw MSS-4 data for the two frames and the processed output on the right. Figure 13 shows the raw and processed data for MSS-5. Some residual effects appear to be present in areas covered by clouds on one of the data sets. These effects are due to cloud shadows, which are not removed by this algorithm, and to the inclusion of marginally clouded pixels which fall within the threshold for cloud detection.

TABLE 1

DEEP WATER STATISTICS FOR MULTITEMPORAL
DATA SET (lines 1730-1750, points 376-426)

	Frame 1889-15033	Frame 5249-14435	Combined Data
MSS4:	mean 45.78	47.99	47.16
	Std.dev. 2.45	1.60	1.47
MSS5:	mean 26.91	26.82	27.02
	Std. dev. 1.84	1.32	1.24
MSS6:	mean 3.77	4.20	4.21
	Std. dev. 0.57	0.71	0.50
MSS7:	mean 0.40	0.46	0.59
	Std. dev. 0.51	0.54	0.53

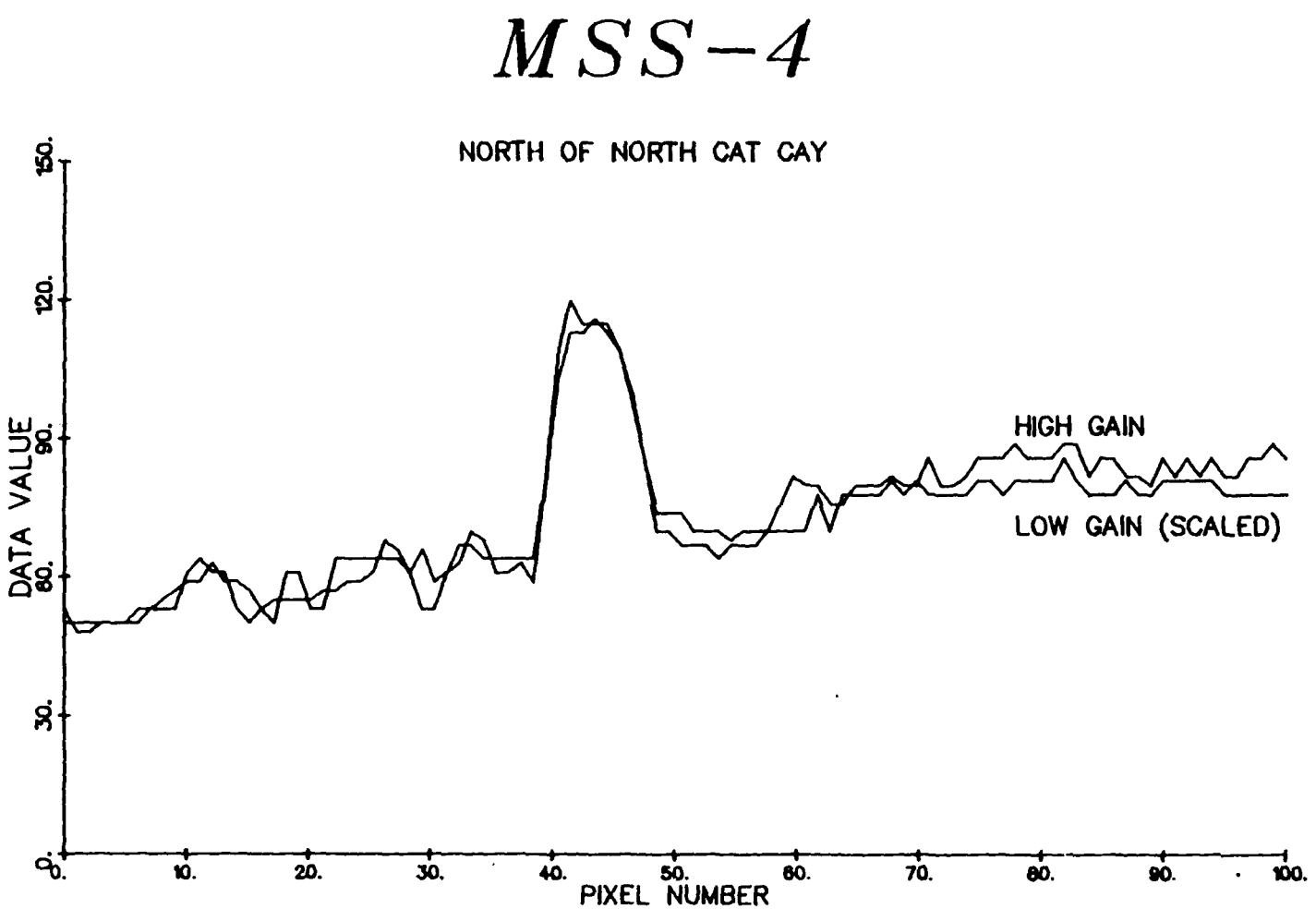

Figure 8. Plots of Scaled Low Gain and High Gain MSS4 Data North of North Cat Cay, Great Bahama Bank.

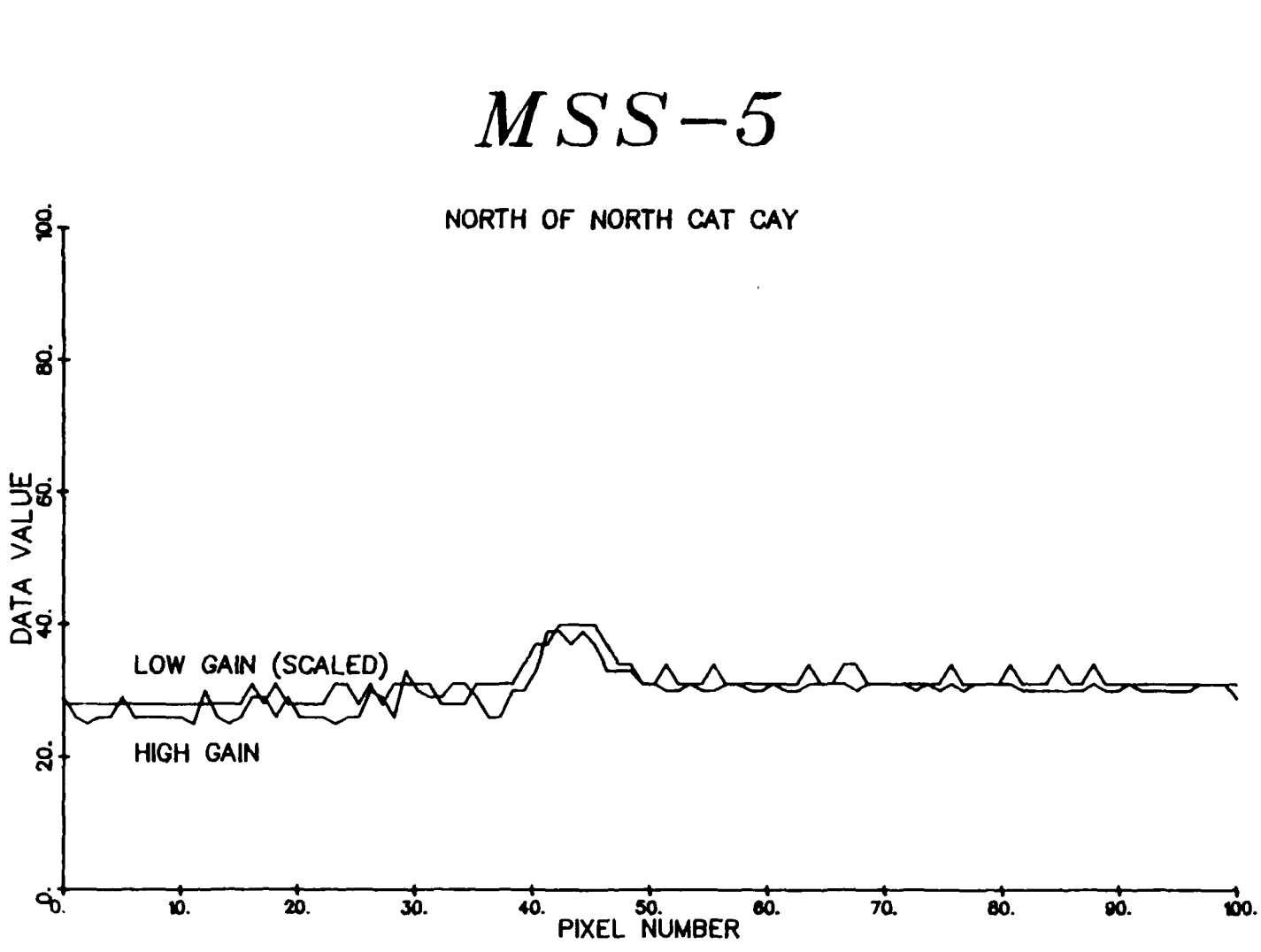

Figure 9. Plots of Scaled Low Gain and High Gain MSS5 Data North of North Cat Cay, Great Bahama Bank

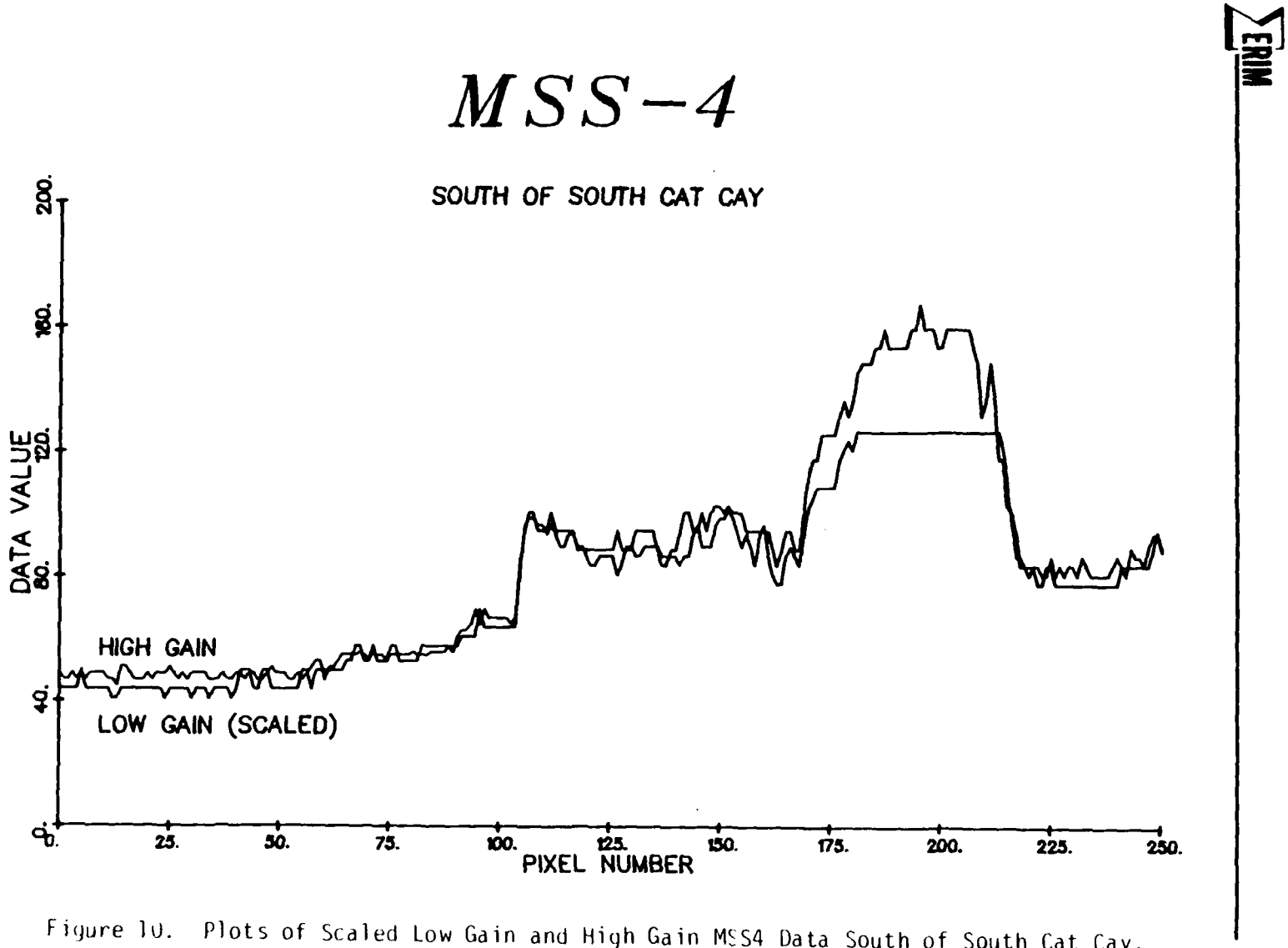

Figure 10. Plots of Scaled Low Gain and High Gain MSS4 Data South of South Cat Cay, Great Bahama Bank

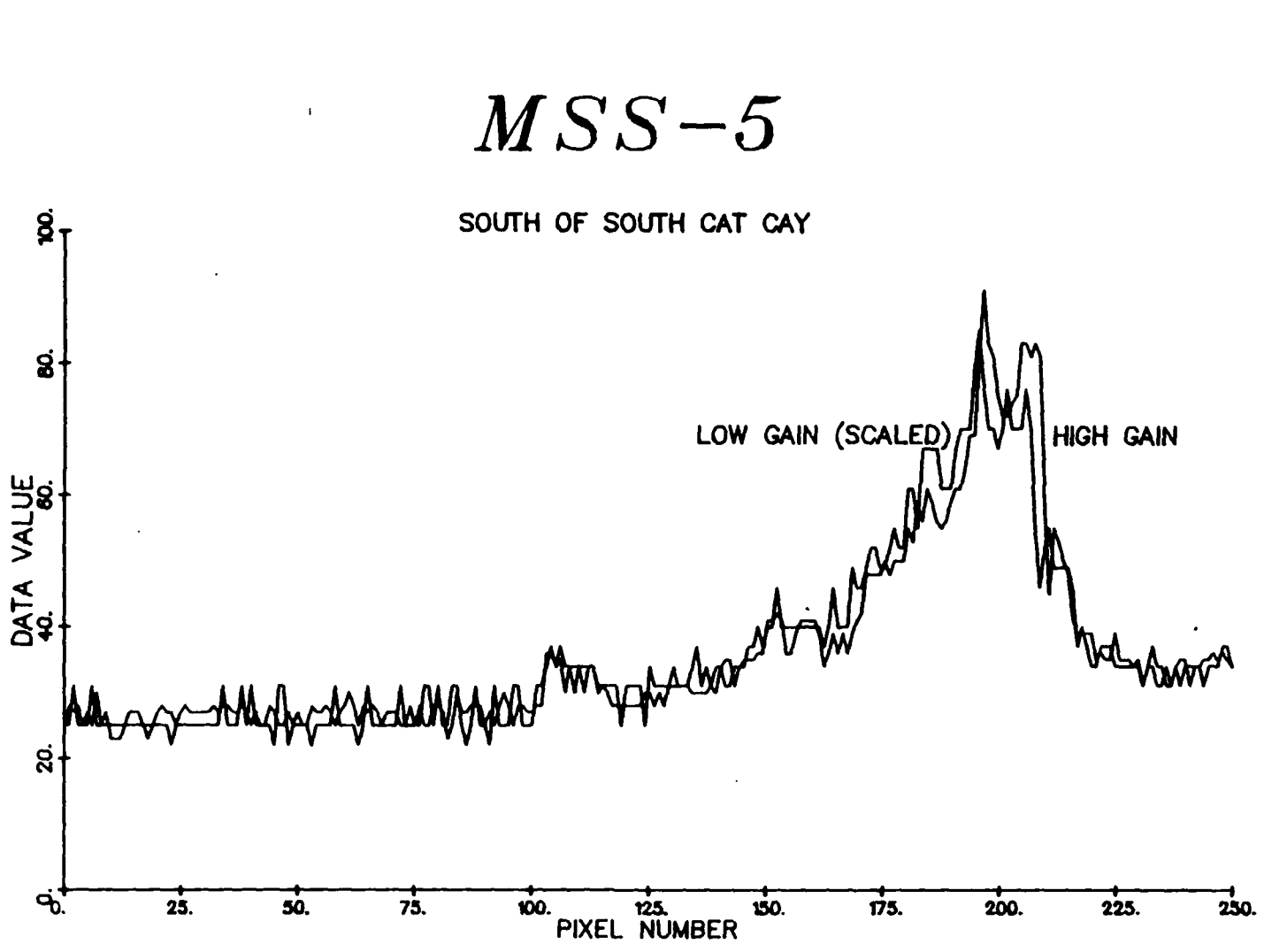

Figure 11. Plots of Scaled Low Gain and High Gain MSS5 Data South of South Cat Cay, Great Bahama Bank

(a) Frame 10889-15033 (Low Gain)

(b) Frame 11249-14435 (High Gain)

(c) Combined Frames, with Transient Suppression

FIGURE 12. B&W IMAGE DISPLAYS OF RAW AND PROCESSED MSS-4 DATA FOR FRAMES 10889-15033 (STRIP 3) AND 11249-14435 (STRIP 3).

(a) Frame 10889-15033 (Low Gain)

(b) Frame 11249-14435 (High Gain)

(c) Combined Frames with Transient Suppression

FIGURE 13. B&W IMAGE DISPLAYS OF RAW AND PROCESSED MSS-5 DATA FOR FRAMES 10889-15033 (STRIP 3) AND 11249-14435 (STRIP 3).

Plots of the multitemporally processed MSS4 and MSS5 data along the same transects north of North Cat Cay and south of South Cat Cay are shown in Figures 14 and 15. A visual comparison with Figures 8-11 shows an apparent reduction in noise, which is confirmed by statistics taken over deep water. These statistics are summarized in Table 1. The standard deviation of the deep water signals for the processed data set is 40 percent lower than that for the scaled low gain data set, and 8 percent lower than that for the high gain data set in MSS4. In MSS5, the improvement is 33 percent over the low gain and 6 percent over the high gain data sets.

Using the criterion that the maximum penetration depth is the depth at which the bottom reflected signal is equal to one standard deviation, the penetration depths for MSS4 are 21.9 meters for the low-gain data set, 24.8 meters for the high gain data, and 25.4 meters for the multitemporal data set. The corresponding figures for MSS5 are 5.6, 6.1, and 6.2 meters, respectively. Deeper penetration can be obtained by spatial filtering, but at the cost of decreasing the spatial resolution. The increased accuracy and penetration depth obtained by multitemporal processing is, of course, accompanied by the benefit of obtaining a cloud-free image.

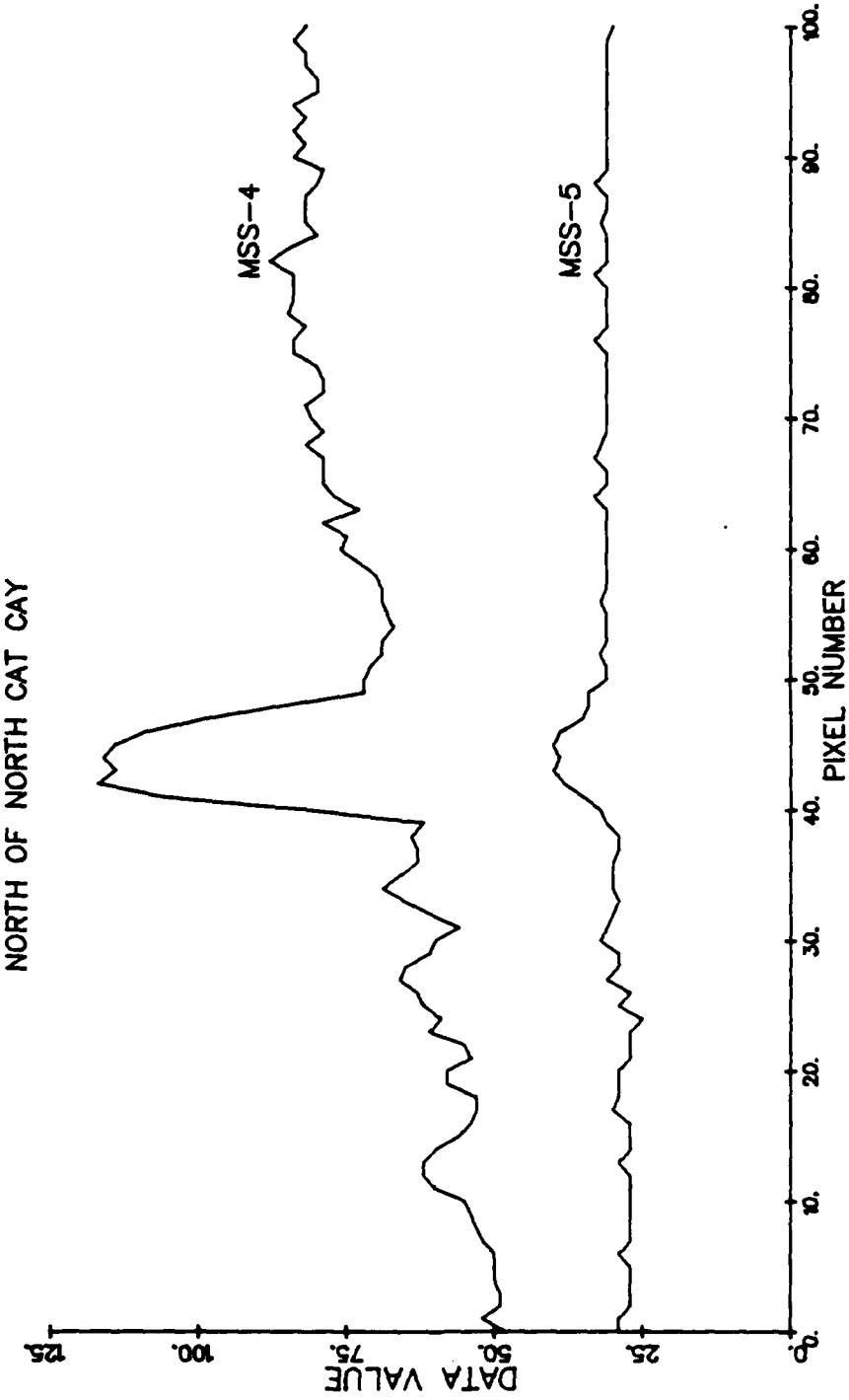

Figure 14. Plots of Multitemporally Processed MSS4 and MSS5 Data North of North Cat Cay, Great Bahama Bank

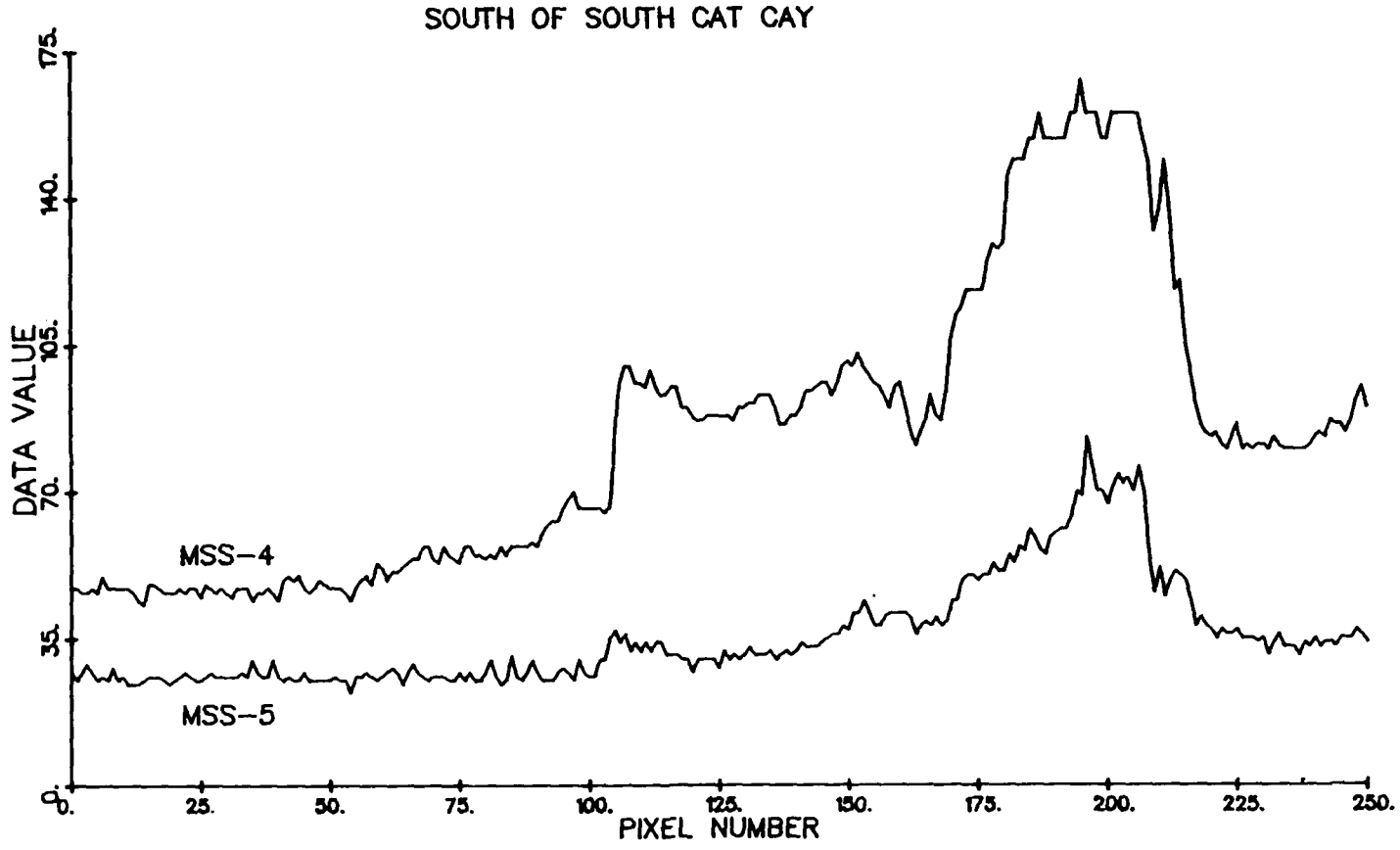

Figure 15. Plots of Multitemporally Processed MSS4 and MSS5 Data South of South Cat Cay, Great Bahama Bank.

7

FIELD VERIFICATION IN THE BAHAMIAN PHOTOBATHYMETRIC CALIBRATION AREA

In order to test the accuracy of the depth extraction methods and to determine the effect of bottom reflectance variations on the depth calculations, a field trip was planned and carried out during October 1977 in the northwestern part of the Great Bahama Bank. The geographic coordinates (latitude and longitude) were determined from satellite navigation equipment aboard ship at 14 achorage locations. Water depths were measured by lead lines and fathometer soundings at each of these locations, and fathometer transects were taken between several of the anchorage locations. In addition, bottom photographs were taken at 18 locations with filters corresponding to Landsat bands MSS-4 and MSS-5 and with a calibrated reflectance standard included in each frame. Of these 18 bottom scenes, 10 were taken at anchorage locations with precise location information and 8 were taken at some distance from the ship. Thus, a complete set of observations (location, depth, and bottom reflectance) were made at 10 stations in the test range. The station numbers, geographic coordinates, and depths for these locations are shown in Table 2.

Bottom reflectances were obtained from the photographs by measuring the density of the film emulsion over each of the three known reflectance panels and using these to plot a curve of film density versus reflectance. An average film density was then measured for the bottom, and the corresponding reflectance was obtained from the calibration curve. The bottom reflectances at each station in the MSS-4 filters are shown in Table 3.

In order to compare the measured depths with those calculated from Landsat data, a set of equations relating the Landsat coordinates to utm coordinates was developed using ground control points supplied by DMA. The geographic coordinates for each station were then converted to utm coordinates using the USGS Transverse Mercator Transformation Program

TABLE 2

LOCATION AND DEPTH OF
TEN STATIONS IN BAHAMA BANK TEST RANGE

STATION NUMBER	LATITUDE	LONGITUDE	DEPTH
C-5	25° 32.20'N	79° 16.92'W	9.8 m
D-7	25° 43.94'N	79° 18.20'W	9.1 m
F-11	25° 56.60'N	78° 59.47'W	9.8 m
G-12	25° 56.36'N	78° 57.77'W	10.4 m
H-13	25° 40.26'N	78° 40.76'W	4.9 m
I-14	25° 40.46'N	78° 42.22'W	6.7 m
J-16	25° 50.48'N	78° 43.82'W	12.5 m
A-17	25° 48.60'N	79° 00.50'W	6.1 m
B-18	26° 01.64'N	79° 05.90'W	10.7 m
D-21	25° 46.15'N	79° 16.73'W	6.1 m

TABLE 3

MEASURED BOTTOM REFLECTANCES AND LANDSAT
SIGNALS IN BAND MSS-4 FOR TEN STATIONS IN BAHAMA TEST RANGE

STATION NUMBER	BOTTOM REFLECTANCE	MSS-4 SIGNAL FRAME 10889-15033	MSS-4 SIGNAL FRAME 11249-14435
C-5	0.20	24	67
D-7	0.24	22	63
F-11	0.23	22	58
G-12	0.19	23	58
H-13	0.24	33	86
I-14	0.10	25	65
J-16	0.10	21	52
A-17	0.23	26	70
B-18	0.15	21	53
D-21	0.16	23	63

No. W5377, and these coordinates were converted to satellite coordinates using the equations described above. This process was repeated for the two Landsat frames mentioned in Section 6 of this report. The utm to satellite coordinate transformation equations for these two frames are as follows:

Frame 10889-15033 (Strip 3):

LINE = 37932 - .002051 (utme) - .01233 (utmn)

POINT = -181 + .01694 (utme) - .003811 (utmn)

Frame 11249-14435 (Strip 3):

LINE = 37882 - .001995 (utme) - .01230 (utmn)

POINT = -252 + .01709 (utme) - .003866 (utmn)

The MSS4 signals at the 10 stations were extracted from both Landsat frames using this procedure, and are listed in Table 3. MSS5 signals were also extracted, but are not listed because they were in most cases not significantly above the deep water signal.

Next, water depths were calculated from the Landsat MSS4 signals for each station, using the procedure described in the NASA/Cousteau report [14]. The water attenuation coefficient was assumed to be that measured during the Cousteau experiment at the Great Isaac Station: i.e. $K_4 = 0.0748\ m^{-1}$. (Water attenuation measurements were also made during the DMA field trip, but because of high sea state at the time of the observations, the measurements were not considered to be representative of normal conditions.) A first order calculation was made using an average (wet) bottom reflectance value of 22 percent for all the stations. This is the same calibration used previously for processing Frame 11249-14435 [15]. The results of these calculations are shown in Table 4. Next, a second order calculation was made using the bottom reflectance values measured for each station. The results of this calculation are shown in Table 5. The equations used for these calibrations are as follows:

$$Z = \frac{-1}{2K} \ln \left(\frac{V-V_s}{V_o-V_s}\right)$$

where $K = 0.0748\ m^{-1}$

$V_o - V_s = 104\ r_b$ for frame 10889-15033

$293\ r_b$ for frame 11249-14435

$V_s = 16.5$ for frame 10889-15033

46.5 for frame 11249-14435

The second order calculation may be viewed as an additive correction to the first order calculation, of the form

$$\Delta Z = \frac{1}{2K} \ln\left(\frac{r_b}{r_b}\right)$$

where r_b is the average bottom reflectance (0.22) used in the first order calculation.

The first order depth calculation miscalculates the depth when the bottom reflectance is different from the average value. However, the second order calculation using the measured reflectances over-corrects for these differences in most cases. The reason for this is probably two-fold: first, at those stations having a partially vegetated bottom (I-14 and J-16) the bottom photogrpahs may have tended to favor the vegetation rather than the sand background, thus yielding a bottom reflectance lower than the average value over the instantaneous field of view of the Landsat sensor. Secondly, the effect of scattering in the water is to reduce the contrast between dark areas and surrounding lighter areas, so that the effective bottom reflectance is intermediate between the actual value within the field of view and those in the surrounding areas. As a result, the r.m.s. error for the second order calculations (2.3 m) is actually larger than that for the first order calculations (1.6 m). The r.m.s. error for the first order corrections is about 18 percent of the average depth for the ten stations.

TABLE 4

FIRST ORDER DEPTH CALCULATIONS FOR TEN STATIONS

STATION NUMBER	FRAME 10889-15033	FRAME 11249-14435	AVERAGE
C-5	7.5 m	7.7 m	7.6 m
D-7	9.5 m	9.1 m	9.3 m
F-11	9.5 m	11.5 m	10.5 m
G-12	8.4 m	11.5 m	10.0 m
H-13	2.2 m	3.3 m	2.8 m
I-14	6.6 m	8.3 m	7.4 m
J-16	10.9 m	16.5 m	13.7 m
A-17	5.9 m	6.7 m	6.3 m
B-18	10.9 m	15.3 m	13.1 m
D-21	8.4 m	9.1 m	8.8 m

TABLE 5

SECOND ORDER DEPTH CALCULATIONS FOR TEN STATIONS

STATION NUMBER	FRAME 10889-15033	FRAME 11249-14435	AVERAGE
C-5	6.9 m	7.1 m	7.0 m
D-7	10.1 m	9.7 m	9.9 m
F-11	9.8 m	11.8 m	10.8 m
G-12	7.4 m	10.5 m	9.0 m
H-13	2.8 m	3.9 m	3.4 m
I-14	1.3 m	3.0 m	2.2 m
J-16	5.6 m	11.2 m	8.4 m
A-17	6.2 m	7.0 m	6.6 m
B-18	8.3 m	12.7 m	10.5 m
D-21	6.3 m	7.0 m	6.6 m

7.1 EFFECTIVE REFLECTANCE DERIVED FROM LANDSAT

To gain further insight into the problem of varying bottom reflectance, the effective reflectance was calculated for each of the 10 sites by assuming the depth was known and solving the depth equation for r_b. Table 6 shows these calculations for both scenes.

For the frame 10889-15033, the measured reflectance as derived from the underwater photograph of the calibration panel agreed with the calculated effective reflectance for the Landsat pixel for 5 of the 10 stations. The remaining cases suggested that at those test sites the measured reflectance was biased by too much vegetation when compared to the size of the Landsat pixel and consequently lower bottom reflectance was reported so that in the second order calculation higher rms errors were introduced.

A similar pattern exists for frame 11249-14435 at 50 percent of the stations, the locally measured reflectance approximates the calculated effective reflectance within a 15 to 20 percent error range. The use of two spectral channel depth calculation algorithms has been shown to be effective in adjusting for these variations in bottom reflectance [15]. Further tests of the effectiveness of bottom reflectance on the accuracy of depth measurements are planned using the data collected in the summer of 1978 in the Bahamas Photobathymetric Calibration range.

A number of data sources including different scale aerial photographs, multispectral active/passive scanner data, and multidate Landsat data will be used to investigate the variable spatial and spectral aspect of this parameter.

TABLE 6

COMPARISON OF MEASURED SUBPIXEL BOTTOM REFLECTANCE AND CALCULATED EFFECTIVE REFLECTANCE FOR A LANDSAT PIXEL

Station Number	Frame 10889-15033(r_b)	Frame 11249-14435(r_b)	Sub-Pixel Measured (r_b)
C-8	.22	.30	.20
D-7	.21	.22	.24
F-11	.23	.17	.23
G-12	.30	.19	.19
H-13	.33	.28	.24
I-14	.22	.17	.10
J-16	.28	.12	.10
A-17	.23	.20	.23
B-18	.21	.11	.15
D-21	.16	.14	.16

REFERENCES

1. W. Richardson and J. Lewis, ERIM Internal Memo IS-WR-197, 3 November 1975.

2. W. Holsztynski, ERIM Internal Memo RI-WH-70, 29 August 1977.

3. N. Rosenberg, A Calibration of Landsat Digital Image Values, submitted for publication, July 1978.

4. Landsat Data Users Handbook, NASA Document No. 765 S4258, 2 September 1976, (supercedes ERTS Data Users Handbook, first published December 1971).

5. V.L. Thomas, Generation and Physical Characteristics of the Landsat 1 and 2 MSS Computer Compatible Tapes, NASA Document No. X-563-75-223, November 1975.

6. P. Van Wie, M. Stein, E. Puccinelli, and B. Fields, Landsat Digital Image Rectification System Preliminary Documentation, Information Extraction Division, Goddard Space Flight Center, November 1975.

7. R.R. Jayroe, Jr., Nearest Neighbor, Bilinear Interpolation and Bicubic Interpolation Geographic Correction Effects on Landsat Imagery, NASA Document No. TMX-73348, September 1976.

8. D.G. Ferneyhough, Jr., and C.W. Niblack, Resampling Study, Final Report, IBM Corporation, March 1977.

9. D.R. Lyzenga, Passive Remote Sensing Techniques for Mapping Water Depth and Bottom Features, Applied Optics 17, 379, 1978.

10. K.R. Piech and J.E. Walker, Aerial Color Analyses of Water Quality, Journal of the Surveying and Mapping Division, ASCE, vol. 97, No. SU2, Nov. 1971.

11. R.E. Turner, Radiative Transfer in Real Atmospheres, ERIM Report No. 190100-24-T, 1974.